A Study on Source Rupture of the 1978 Lan-Hsu, Southeastern Taiwan Earthquake

NIEN-PING CHOU [1,2] AND JEEN-HWA WANG [1]

ABSTRACT

Seven teleseismic long period P-wave records from World-Wide Standard Seismograph Network (WWSSN) are used to infer the source rupture process of the July 23, 1978 Lanhsu, eastern Taiwan earthquake through the body-wave iterative deconvolution method (Kikuchi and Kanamori, 1982; 1986). Results show that the rupture sequence consists of one main event and one largest subevent near the hypocenter determined by Pezzopane and Wesnousky (1989) and numerous smaller ones at a distance from the hypocenter. Comparison of the spatial distribution of mainshock rupture sequence with aftershocks shows that aftershocks are located in the area which did not break before the occurrence of the above-mentioned events. The total seismic moment of the three largest events is 8.76×10^{26} *dyne-cm*.

1. INTRODUCTION

Taiwan is located at the convergent boundary of the Eurasian and Philippine Sea plates. It is proposed that the Eurasian plate subducts southeastward beneath the Philippine Sea plate at about 21.5° *N* along the Manila Trench, whereas the Philippine Sea plate subducts northeastward beneath the Eurasian plate along the Ryukyu trench at 23.5° *N* (Tsai, 1986). For the past 4 million years, the collision between the Luzon island arc and the Chinese continental margin of the northern Eurasian plate has resulted in folded thrust sheets in central Taiwan and volcanic arc in the eastern coast of Taiwan. The Longitudinal Valley fault is assumed to be the suture of the arc-continent collision (Barrier and Angelier, 1986).

On July 23, 1978, an earthquake ($M_L = 6.8$, $m_b = 6.5$, $M_s = 7.4$) took place about 20 *km* northwest of the Lanhsu island in the southeastern offshore of Taiwan (Lee and Tsai, 1981). From the data of the Taiwan Telemetered Seismographic Network (TTSN), it is located at 22°21.11' *N* and 121°19.72' *E* (see Figure 1a) and its focal depth is 6.1 *km*. The hypocenter determined by Lee and Tsai is named as LT hypocenter in this work. Lee and Tsai (1981) reported that about one and a half years before the mainshock, microearthquake activity remarkably increased in number and clustered in the space toward the ensuing focal zone.

[1] *Institute of Earth Sciences, Academia Sinica, Taipei, R.O.C.*

[2] *Institute of Geophysics, National Central University, Chungli, Taiwan, R.O.C.*

Since the mainshock, microearthquake activity in the area has returned to the background level. The aftershock zone during the first nine days following the mainshock was about 60 *km* long in the NS direction, 20 *km* wide in the EW direction and 40 *km* deep. Moreover, 72 shocks with $M_D > 4.0$ were confined to a smaller zone, called the main rupture zone of $30 \times 15 \times 10$ km^3. The mainshock, located at the northern end of this main rupture zone, and some larger aftershocks have strike-slip fault focal mechanisms. Giardini *et al.* (1985) determined the source mechanism of this earthquake through the centroid-moment-tensor method. Pezzopane and Wesnousky (1989) used generalized ray theory to invert the source rupture process. The hypocenter determined by Pezzopane and Wesnousky is named the PW hypocenter in this work. The focal mechanisms and source parameters reported by these authors are listed in Table 1 and shown in Figure 1b.

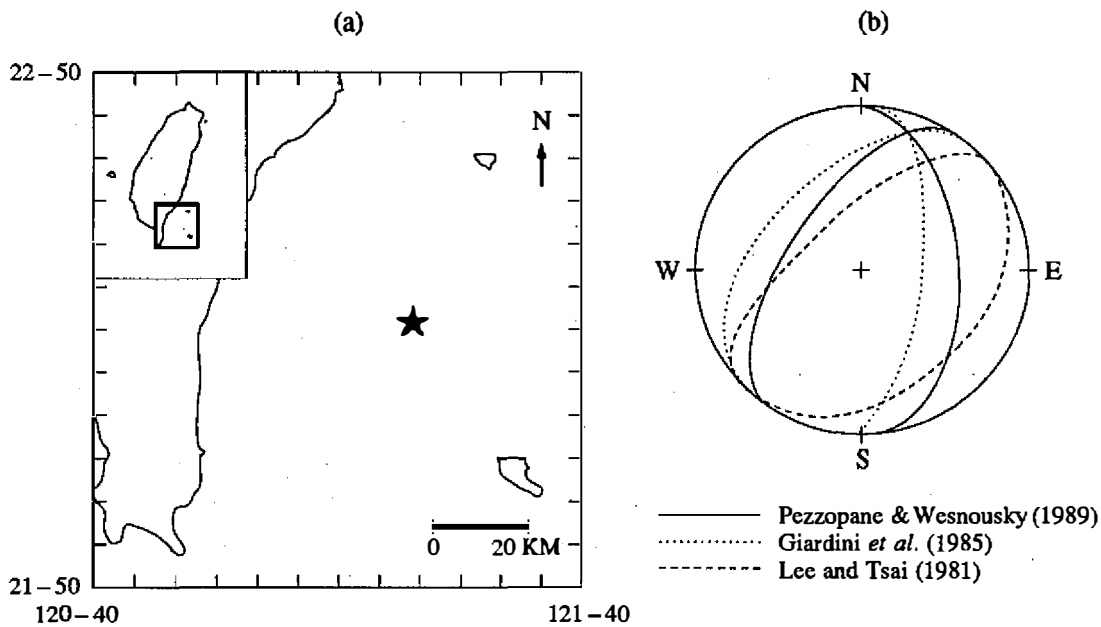

Fig. 1. (a) The location of July 23, 1978 Lanhsu earthquake and its surrounding area. The 'solid star' denotes the epicenter. (b) Fault plane solutions of the Lanhsu earthquake: dash lines by Lee and Tsai (1981), solid lines by Pezzopane and Wesnousky (1989), and dotted lines by Giardini *et al.* (1985).

Table 1. Source parameters

authors	strike angle	dip angle	rake angle	depth (*km*)	seismic moment ($\times 10^{26}$ *dyne-cm*)
Lee and Tsai (1981)	48°	27°	0°	6.1	
Pezzopane and Wesnousky (1989)	355°	42°	62°	26	4.6
Giardini *et al.* (1985)	5°	61°	69°	28.9	8.64

Since this earthquake was near the collision boundary of the Eurasian and Philippine Sea planes, it is significant to invert the distribution of mechanical properties in the source area to infer its relevance to regional tectonics. In this study, a body-wave iterative deconvolution method will be used to invert the source space-time function.

2. METHOD

The inversion technique of body-wave iterative deconvolution method used in this study was developed by Kikuchi and Kanamori (1982 and 1986) and Kikuchi and Fukao (1985 and 1987). The source process is described as a sequence of point dislocations, each being characterized by seismic moment (m_i), onset time (t_i) and coordinates (x_i, y_i) on the fault plane, where we take the x-axis along the fault strike and the y-axis along the dip. The considered fault plane is divided into $n_x \times n_y$ grids, and adjacent two grid points are separated by Δx in both x- and y-directions. The fault mechanism and source time history are assumed to be identical for all point sources. The synthetic wavelet (i.e. Green function) at the j-th station, generated from a unit point source (x_i, y_i) at time t_i, is denoted by $W_j(t_i; x_i, y_i)$, and the synthetic record generated from a point source (m_i, t_i, x_i, y_i) is represented as $m_i W_j(t_i; x_i, y_i)$. In the first iteration, the point source (m_1, t_1, x_1, y_1) is determined through the minimization of the error:

$$\Delta = \sum_{j=1}^{M} \int \left[X_j(t) - m_1 W(t - t_1; x_1, y_1) \right]^2 dt \tag{1}$$

where $X_j(t)$ is the observed seismogram at the j-th station, the time t is measured from the initial arrival at each station, and M is the total number of stations. In the next step, the observed waveform in Eq. (1) is replaced by the residual waveform:

$$X_j'(t) = X_j(t) - m_1 W_j(t - t_1; x_1, y_1) \tag{2}$$

The point source parameters (m_2, t_2, x_2, y_2) are determined by Eq. (2) through the same procedure as above. Thus, after N iterations, we obtain N point source parameters (m_i, t_i, x_i, y_i), $i = 1, 2, \ldots, N$. The resultant synthetic waveform is given by:

$$Y_j(t) = \sum_{i=1}^{N} m_i W(t - t_i; x_i, y_i) \tag{3}$$

The moment rate function $\dot{M}_0(t)$ and total seismic moment M_o are given as:

$$\dot{M}_0(t) = \sum_{i=1}^{N} m_i u_i(t - t_i) \tag{4}$$

and

$$M_o(t) = \sum_{i=1}^{N} m_i \tag{5}$$

where $u_i(t)$ is the source time function of an individual source with a unit seismic moment. Through the above procedure, the temporal-spatial distribution of each point source is iteratively determined.

3. DATA

The vertical-component records of teleseismic long-period P-waves at seven WWSSN stations have been analyzed. The epicentral distances are ranged from 30° to 90° to avoid the complicated phases from the crust and upper mantle and the diffracted phases from the core-mantle boundary. The related parameters for the seven stations are listed in Table 2. The seismic signal has been filtered by instrument and affected by the local geological structure near station, especially for the later-arriving phases. Hence, only few motions of the record have been taken into account for the reliability of data. A far field waveform can be represented as:

$$U_c(\bar{x},t)=\frac{1}{4\pi\rho c^3}\left(\frac{R_c}{r_o}\right)S(t) \tag{6}$$

where ρ, c, $S(t)$ are density, velocity and far-field source time function respectively. The first-motion amplitude is proportional to (R_c/r_o), where R_c is the radiation pattern in terms of fault parameters, take-off angle of the seismic ray and azimuth angle of the station (Aki and Richards, 1980). The observed first-motion amplitudes and calculated values from the three fault plane solutions determined by Pezzopane and Wesnousky (1989), Giardini *et al.* (1985) and Lee and Tsai (1981) are shown in Figure 2. It can be found that the variation of amplitude with distance of the observed data is similar to those of calculated data under the parameters by Pezzopane and Wesnousky (1989) and Lee and Tsai (1981) in spite of the match of the values of amplitude, but does differ from that under the parameters by Giardini *et al.* (1985). The fault plane solution, determined by Giardini *et al.* from the seismograms of periods from 45 to 135 *sec.*, shows the long-period source mechanism. Thus the fault plane solution determined by Giardini *et al.*(1985) might not be an appropriate initial model for the inversion of source ruptures from the short-period data by the Kikuchi and Kanamori's technique. The values of differences between the observed amplitudes and the two calculated ones from the Pezzopane and Wesnousky's as well as the Lee and Tsai's parameters are in the range of 0.15 to 0.40.

For practical computation, it is important to take an adequate segment of seismograms for each station to cover all of the *P*, *pP* and *sP* phases generated from all of the point sources during the source rupture but it should include the other reflected and refracted phases. Unfortunately, there is not any definite way to determine source rupture duration before the inversion procedure. The only approximate way is to estimate it from earthquake magnitude. We, therefore, proposed that larger earthquakes should have longer duration time. As some previous studies suggested (Kikuchi and Fukao 1985; 1987), the main subevents are expected to happen within 20 *seconds* after the initial rupture for an earthquake with seismic moment in order of 10^{26} *dyne-cm*. After further consideration of the

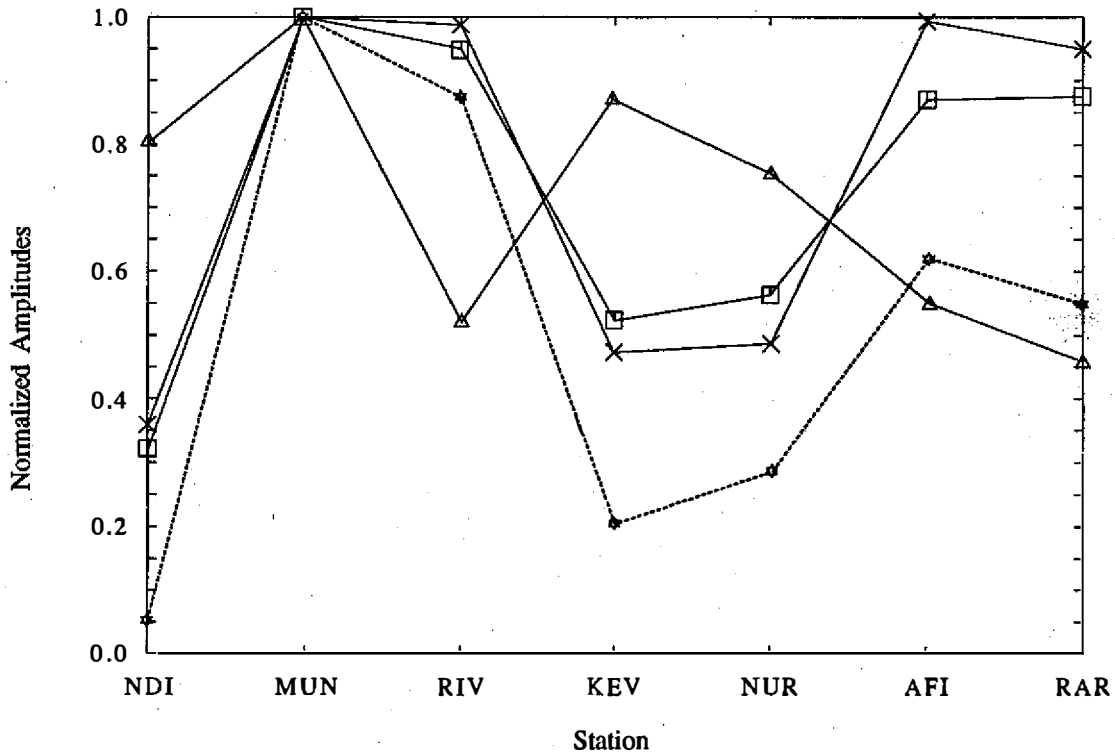

Fig. 2. Observed and calculated first-motion amplitudes normalized with respect to that at station MUN: dotted line for observed data and solid lines for calculated values (square, cross and triangle symbols denote the values based on the focal parameters by Lee and Tsai (1981), Pezzopane and Wesnousky (1989), and Giaridini *et al.* (1985), respectively).

Table 2. Station parameters

station code	azimuth (degree)	epicentral distance	magnification	ray parameter (*sec / km*)	geometrical spreading (10^{-5} / *km*)
Pacific stations					
AFI	112°	74.6°	750	0.046	4.74
RAR	114°	88.1°	375	0.045	4.00
RIV	152°	62.2°	750	0.062	5.50
MUN	185°	54.1°	375	0.064	6.28
Eurasian stations					
NDI	289°	40.3°	1500	0.075	7.16
NUR	329°	74.2°	1500	0.049	4.74
KEV	338°	70.9°	1500	0.056	4.90

travel time of the *sP* phase, a 60-*second* rupture duration was selected.

The difference in the arrival times between the second phase (*pP* phase) and the first phase (*P* phase) and that between the third phase (*sP* phase) and the first phase (*P* phase) were measured. The former is denoted by $\Delta T_p pp$ and the latter by $\Delta T_s pp$. The measured $\Delta T_p pp$ and $\Delta T_s pp$ values are from 10.8 *sec.* to 20.8 *sec.* and from 27.0 *sec.* to 42.0 *sec.* They are shown in Figure 3. For $\Delta T_s pp$, the values at European stations (NDI, KEV and NUR) are about 10 *sec.* smaller than those at Pacific stations (MUN, RIV, AFI and RAR). For $\Delta T_p pp$, the values at two Pacific stations (MUN and RIV) with smaller epicentral distances are about 10 *sec.* larger than those at European stations, while the values at two Pacific stations (AFI and RAR) with larger epicentral distances are only about 5 *sec.* larger than those at European stations.

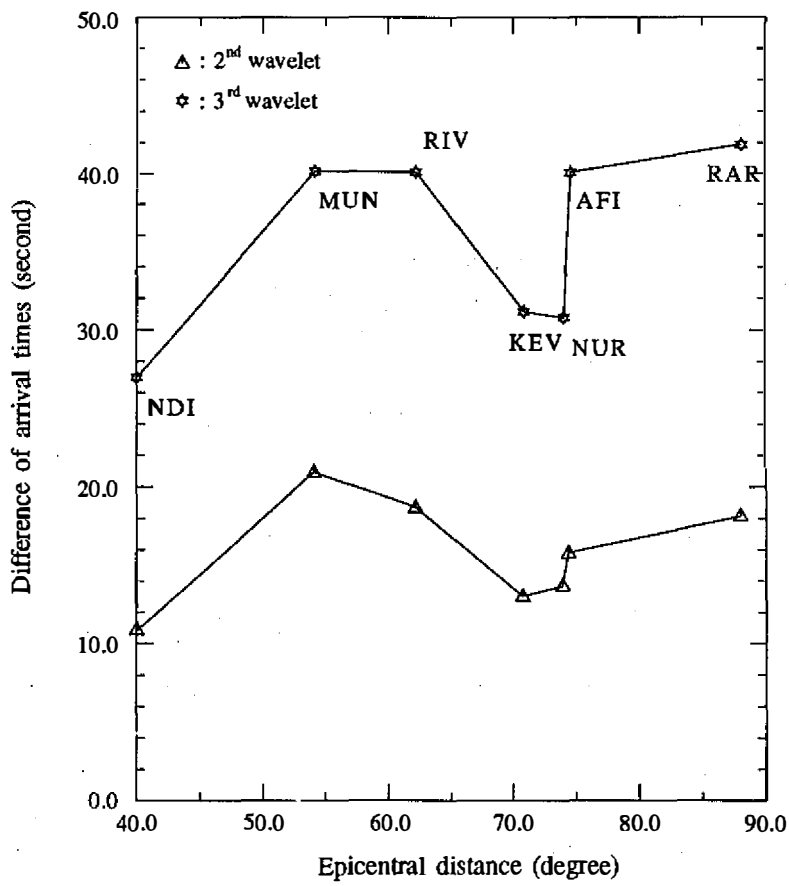

Fig. 3. Differences of arrival times of the second and third wavelets with respect to that of the first wavelets observed at seven stations NDI, MUN, RIV, KEV, NUR, AFI and RAR (from left to right).

4. MODELS

Before iteration, the initial model must be first constructed. Since the dominant periods of the seismograms used ranged from 15 to 27 *sec.*, the fault-plane solution obtained by Giardini *et al.* (1985), which is based on the seismograms with periods greater than 40 *sec.*, is not used. The two initial fault-plane models used are determined by Lee and Tsai (1981) and Pezzopane and Wesnousky (1989). Their geometric structures are shown in Figure 4. The area of the fault planes are inferred from the aftershocks. Totally, 18×12 and 12×12 grid points with an equal spacing of 5 *km* are defined for the two models to include all aftershocks under distinctive fault plane solutions. Time history of individual subevent is a trapezoid time function with two time constants: rise time and rupture duration, which are determined by Pezzopane and Wesnousky (1989).

For far-field waveform synthesis, the geological structure is simplified to a half-space. The rupture velocity is taked as 3.4 *km / sec*, which is about 0.9 times of half-space S-wave velocity of the source area.

5. RESULTS

The Kikuchi and Kanamori's inversion method can be used for both single-station data and multi-station data. In this work, we study the source mechanism as inverted first through the single-station inversion, then through the multi-station inversion.

Single-station inversion

The iteration errors for the seven stations through the single-station inversion based on Lee and Tsai's model are shown in Figure 5a. The errors reduce rapidly during the first five iterations, then become essentially constant after the sixth iteration. The least error is for station MUN, and the largest error is for station NDI. Figure 6 shows the observed seismograms and synthetic seismograms, source time functions, and spatial distributions of subevents for the seven single stations. A remarkable distinction between the results for

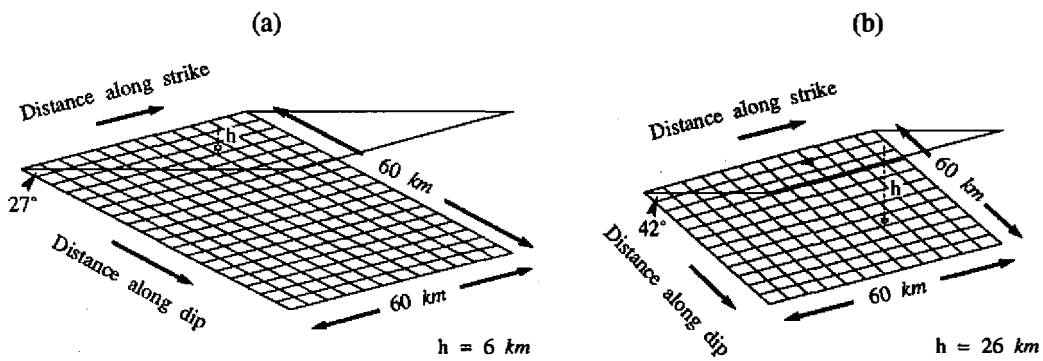

Fig. 4. Geometry of models: (a) based on Lee and Tsai's source parameters and (b) based on Pezzopane and Wesnousky's source parameters.

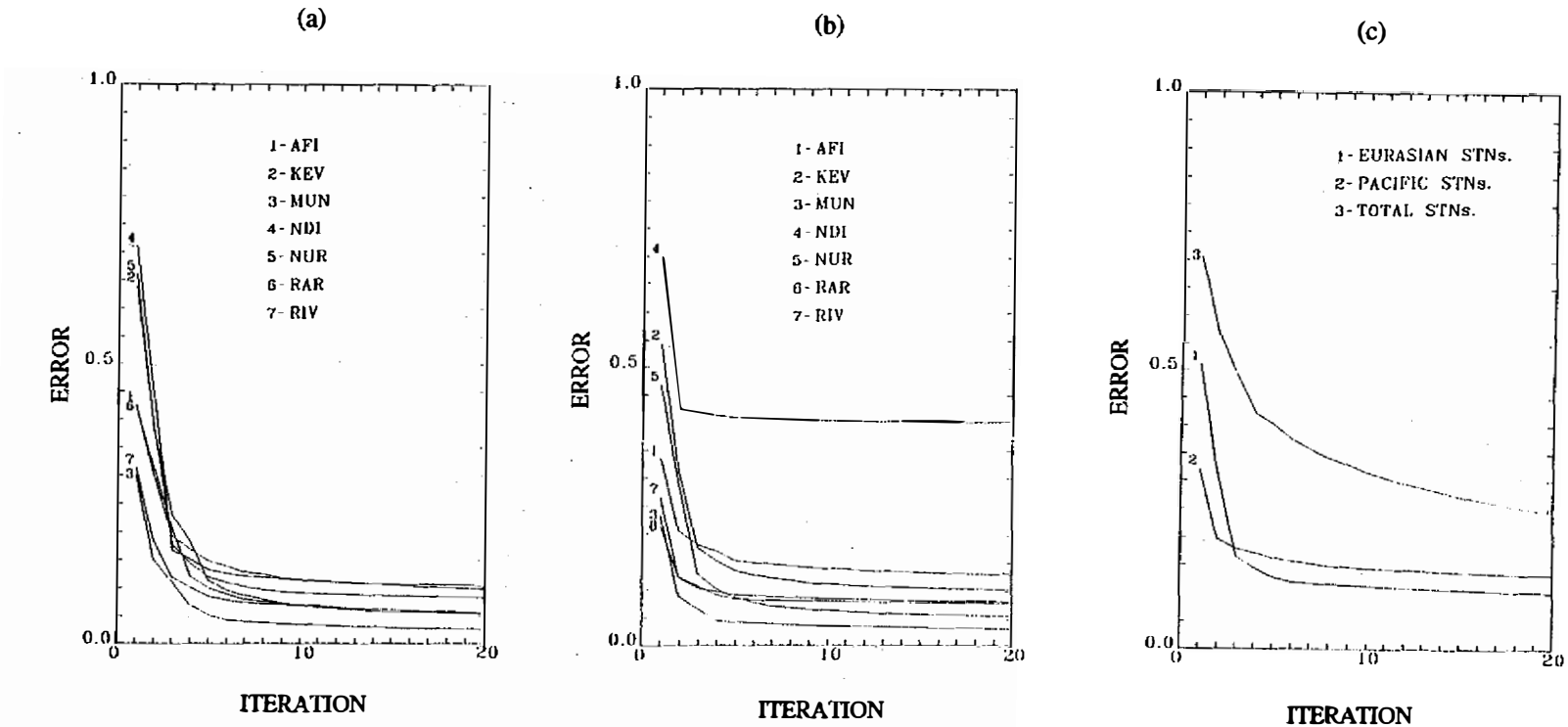

Fig. 5. Variations of error with iteration: (a) for seven stations through single-station inversion based on Lee and Tsai's source parameters; (b) for seven stations through single-station inversion based on Pezzopane and Wesnousky's source parameters; (c) for Pacific stations, Eurasian stations and all stations through multi-station inversion based on Pezzopane and Wesnousky's source parameters.

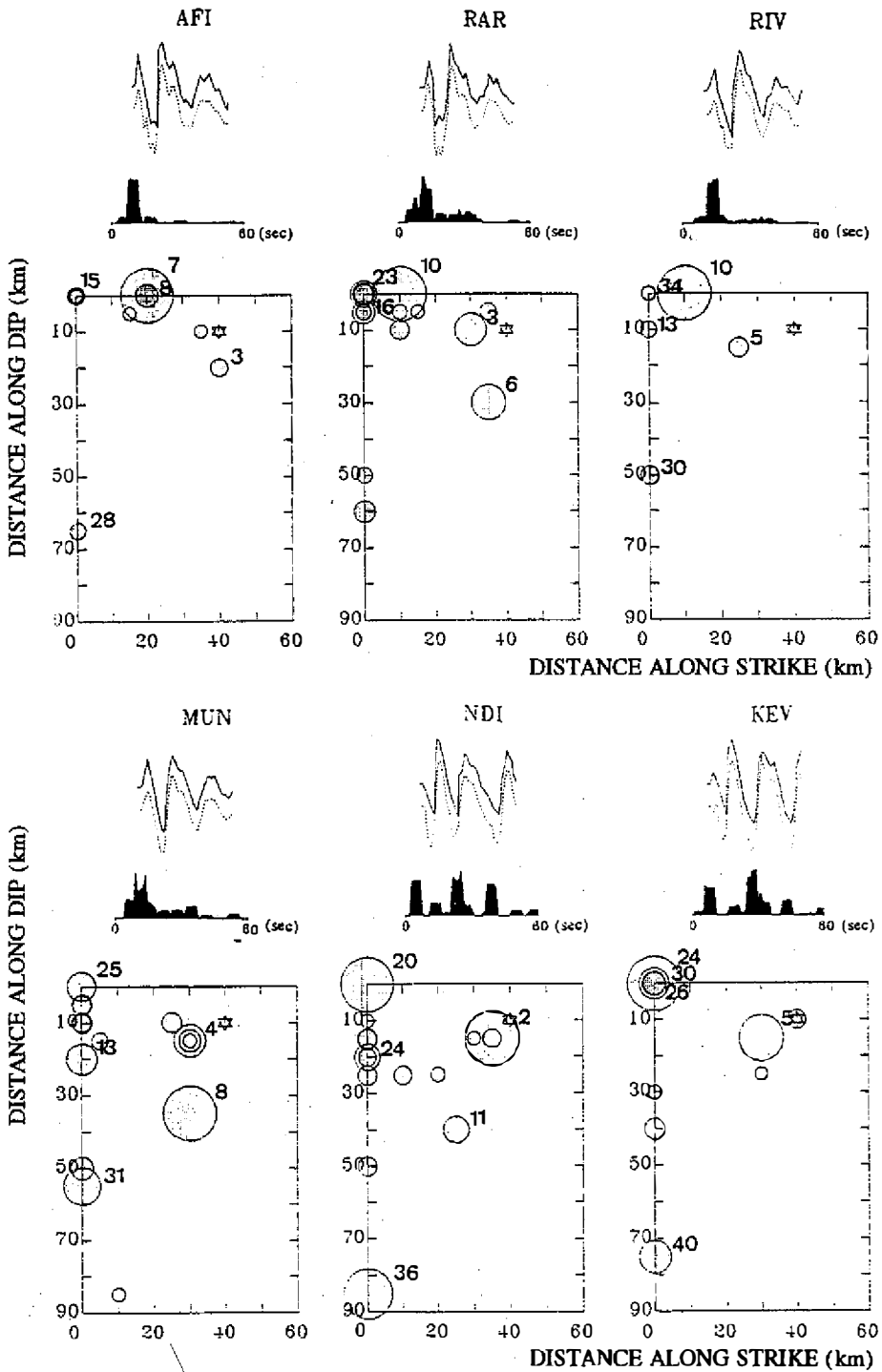

Fig. 6. Temporal-spatial distributions of subevents and relative source time functions for seven stations based on Lee and Tsai's model through single-station inversion. The observed and synthetic seismograms are denoted by solid and dashed lines. The subevents are denoted by shaded circles with a number denotes the onset time of greatest five rupture events. The asterisk marks the position of hypocenter.

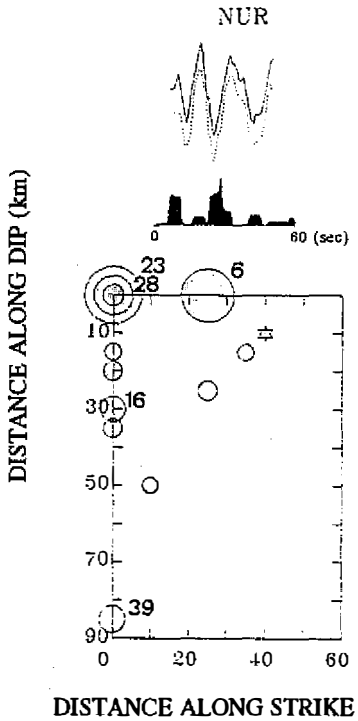

Fig. 6. Continued.

Pacific stations and those for the Eurasian stations can be delineated. Results for Pacific stations are characterized by a large event at the time of about 10.0 *sec.*, whereas those for Eurasian stations are specified by two large events at about 5.0 and 24.0 *sec.* Besides, the first-motion polarities of the synthetic seismograms at Eurasian stations are opposite to those of the observed ones. The spatial distribution of subevents shows that their initial ruptures mostly depart from the LT hypocenter, and larger events are set in the boundary grids, where the lowest reliability of the results should be made. From these doubtful results, we would not perform the multi-station inversion for Lee and Tsai's model.

Figure 5b shows the iteration errors for the seven stations through the single-station inversion based on the Pezzopane and Wesnousky model. The errors are reduced in a similar way to those based on the Lee and Tsai model, but the final errors are higher than those based on the latter model. The errors for station NDI are 0.4 after the second iteration. The source rupture from the seismogram of this station cannot be inverted on the basis of the Pezzopane and Wesnousky model. Results from the single-station inversion are shown in Figure 7. The synthetic seismograms fit the observed seismograms very well except that of NDI. The distinction between the results from Pacific stations and those from Eurasian stations still exists. However, the temporal-spatial distributions of events inferred from the data of Pacific stations based on this model seem to be more reasonable than those based on Lee and Tsai's model because they fit the constraint of afterschocks area better, and the initial events are concentrated in the vicinity of the determined hypocenter, as we expected.

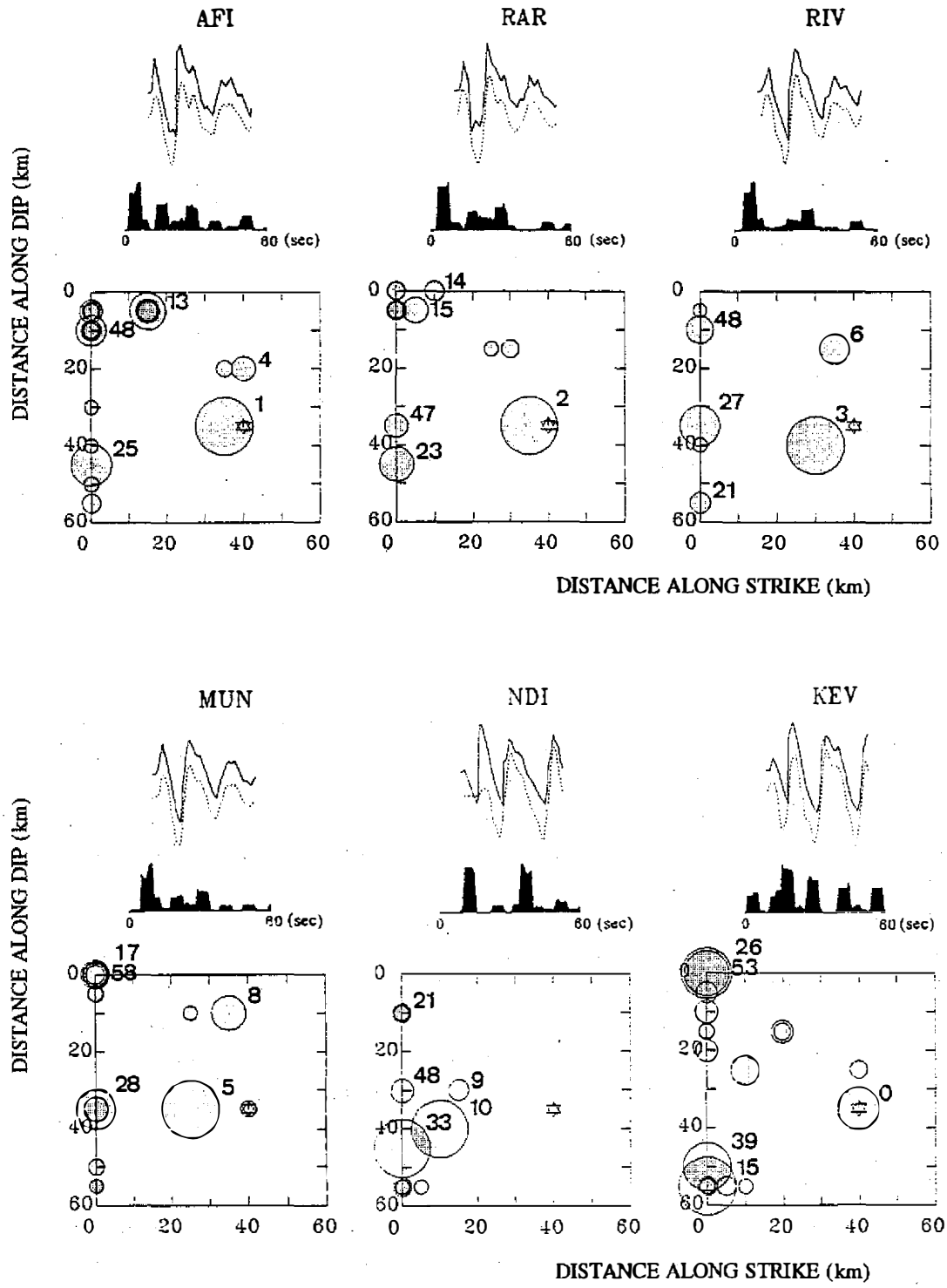

Fig. 7. Temporal-spatial distributions of subevents and relative source time functions for seven stations based on Pezzopane and Wesnousky's model through single-station inversion.

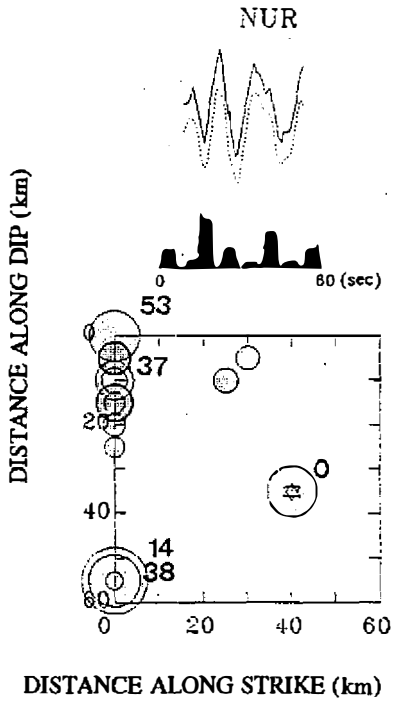

Fig. 7. Continued.

The figure shows only one larger event in the temporal sequence for each Pacific station. The occurrence times of such larger events are within 1.0 to 5.0 *sec.* On the other hand, several larger events are inverted from the data of Eurasian stations. The source time functions and the size of the largest subevent from the data of Eurasian stations are different from those of Pacific stations. However, their spatial patterns of subevents are somewhat similar. The spatial patterns of subevents show that the first subevent, which is the largest one, is near the PW hypocenter, and several smaller and later-occurring subevents are in the southern part (or the left-hand side on Figure 7) of the fault plane. Those later-occurring subevents can be separated into two groups, one in the shallow zone and the other at depth. The subevents of the group at depth are, in general, larger than those in the shallow zone.

The seismic moments for subevents inverted after 20 iterations are listed in Table 3. The seismic moments obtained from the data of Pacific stations are almost half of those obtained from the data of Eurasian stations, and 3.5 times of that reported by Pezzopane and Wesnousky (1989) and 1.8 times of that by Giardini *et al.* (1985).

Multi-station inversion

In the single-station inversion, the distinction between the results from the data of Pacific stations and Eurasian stations is obvious. Therefore, we have performed inversions for these two individual data sets and finally a joint inversion for all of these data. Among the data, as mentioned before, the fitting of synthetic seismograms with observed ones at NDI aren't good, and we have therefore excluded the data of this station for the multi-station inversion. The iteration errors for the multi-station inversions are shown in Figure

Table 3. Seismic moments inverted from individual seismograms at seven stations

Station code	Seismic moment ($\times 10^{27}$ *dyne-cm*) Lee and Tsai	Pezzopane and Wesnousky
Pacific stations		
AFI	40.4	1.56
RAR	3.11	1.34
RIV	3.53	1.56
MUN	1.98	1.87
Eurasian stations		
NDI	3.76	1.54
NUR	6.49	3.31
KEV	4.80	3.08

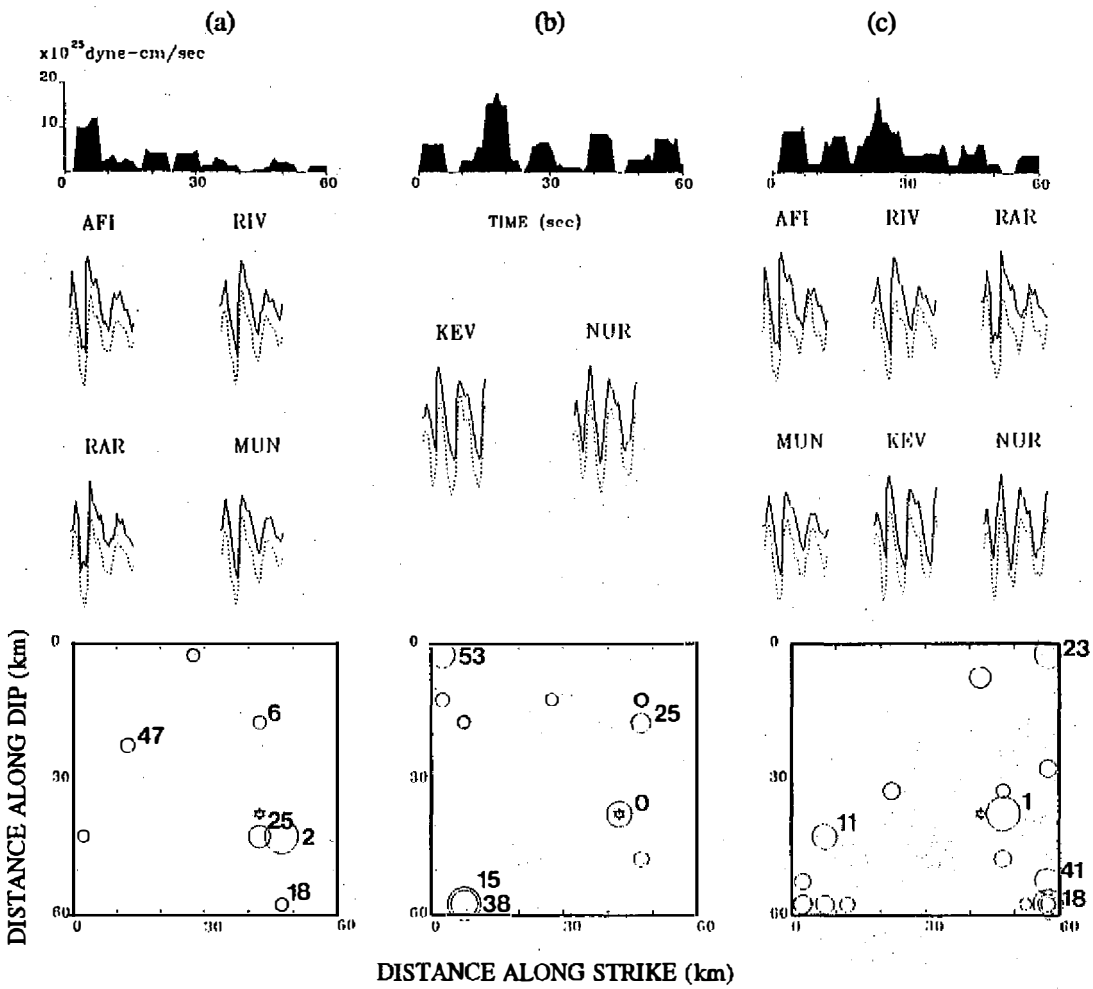

Fig. 8. Temporal-spatial distributions of subevents based on Pezzopane and Wesnousky's model through multi-station inversion: (a) for the data of four Pacific stations; (b) for the data of two Eurasian stations; (c) for six data described by (a) and (b).

5c. The errors for the two individual sets are approximately constant (about 0.15) after 5 iterations, but the error for the joint data decreases with the number of iteration and is about 0.25 after 20 iterations. Inverted results are shown in Figure 8. The spatial pattern of subevents from the data of Pacific stations is similar to those from each data set of these stations by single-station inversion. Both results show that a main subevent occurs first after 2.0 *sec.* followed by five smaller subevents. Two larger subevents are located near the PW hypocenter, and smaller ones are distributed over the fault plane. The spatial pattern inverted from the data set of Eurasian stations shows that three subevents occur at 15.0, 38.0 and 53.0 *sec.* Comparison of Figure 7 and Figure 8b shows that the source time function in the multi-station inversion is an average superposition of those in single-station inversions of the data of KEV and NUR. This phenomenon is particularly remarkable in the case of joint data inversion (i.e. Figure 8c).

Results show that some large multi-rupture events appear at the boundary grids. Since the area of each grid is 25 km^2, it is impossible to accumulate enough energy for multi-ruptures in such a small area within a short period of time. So, we have extended the fault plane to a larger size, such as 100×60 km^2, then resumed the inversion. The result is shown in Figure 9, in which the prescribed boundary events remarkably move along the direction of boundary extension. It indicates an existing error in the inversion of spatial distribution caused by the requirement of matching the synthetic waveform with the observed one. This error will be reduced when the fault plane is extended, but an unreasonable inversion results. So the inversion results for the boundary events are less reliable.

Figure 10 shows the variations of inverted seismic moment with the number of iterations for Pacific and Eurasian data sets. For Pacific data set, the seismic moment almost monotonically decreases with iteration. A similar variation also exists for Eurasian data set except for the appearance of an abnormal value at the sixth iteration. Before the seventeenth iteration, the values of seismic moment from Pacific data set are smaller to those from Eurasian data set, but vice verse after the seventeenth iteration. However, after the tenth iteration, the values of seismic moment from the two data sets are very similar.

6. DISCUSSION

The spatial pattern of subevents inverted from the data of Eurasian stations (Figure 8b) is more complicated than that from the data of Pacific stations (Figure 8a). One possible reason for this distinction is due to the different crustal structures of these two regions: a continental type for Eurasian stations and an oceanic type for Pacific stations. In general, the oceanic crust has a thickness of about 5 to 10 *km*, while the continental crust has a thickness of about 30 to 80 *km*. The travel times of body waves would be different within the two crusts. Besides, the continental crust composition is more complex than the oceanic crust. The former consists of two main layers: the upper layer with granite and the lower layer with basalt; in contrast, the latter is essentially a layer of basalt. The shallow part of the continental crust is quite complicated and may be composed of nonflat structures. However, this shallow part is not thick and does not have a remarkable influence on the intermediate-

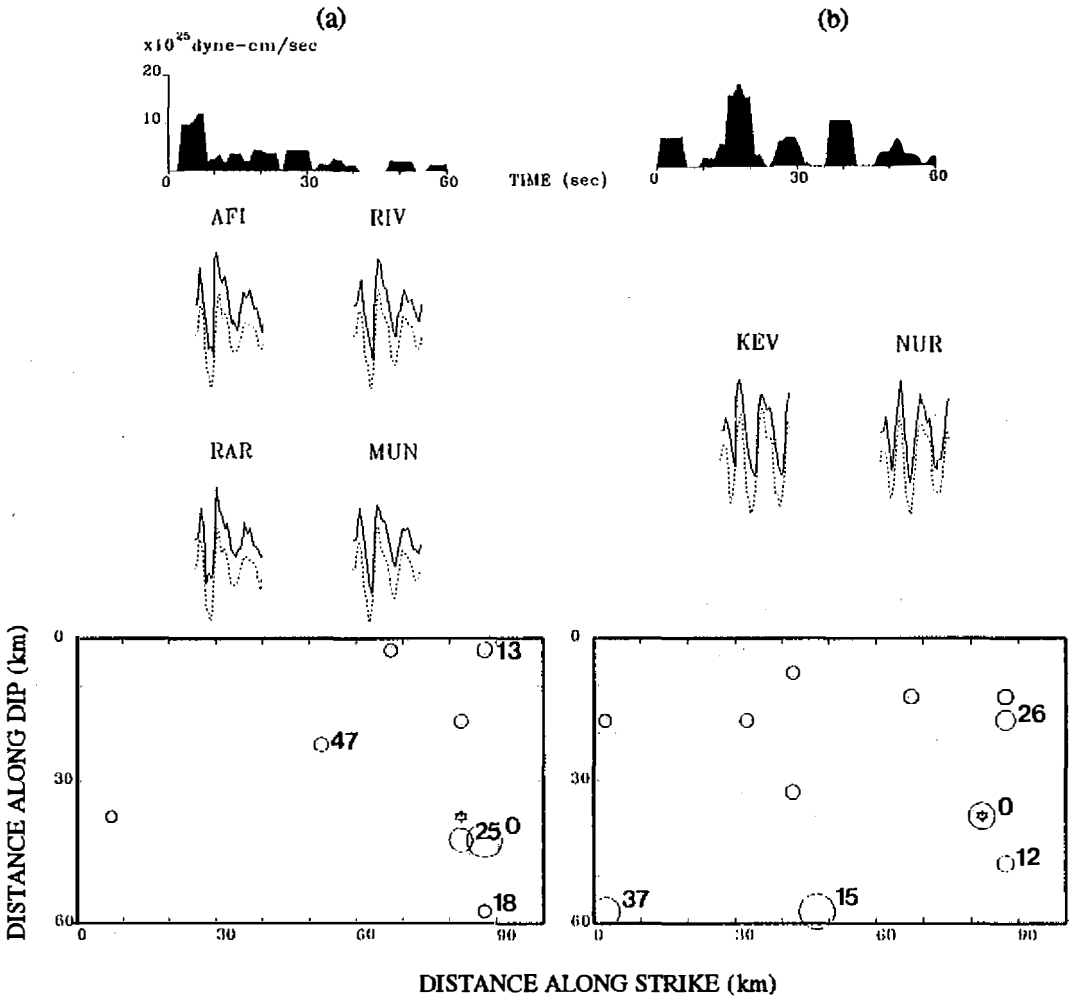

Fig. 9. Temporal-spatial distributions of subevents through multi-station inversion for extended source area with dimension of $100 \times 60\ km^2$ from Pezzopane and Wesnousky's model: (a) for four Pacific stations and (b) for two Eurasian stations.

period body waves used in this study. The difference between the occurrence times of the first and largest subevent in time history of Figure 8a and the second and largest subevent in time history of Figure 8b is about 10 *sec.*, which is related to a ray path of P waves of 50 *km* as the average P wave velocity of the crust is considered to be 5 *km/sec.* The value of 50 *km* is approximately equal to the difference in thicknesses of the continental and oceanic crusts.

From Table 3, the resultant seismic moments after 20 iterations are larger than those reported by other authors (e.g. Pezzopane and Wesnousky, 1989; Giardini *et al.*, 1985). In our inversion process, all the data recorded in the truncated seismogram are deemed to be generated directly from the source rupture. However, some refracted and reflected signals might exist. These signals would yield small subevents, thus increasing the heterogeneity

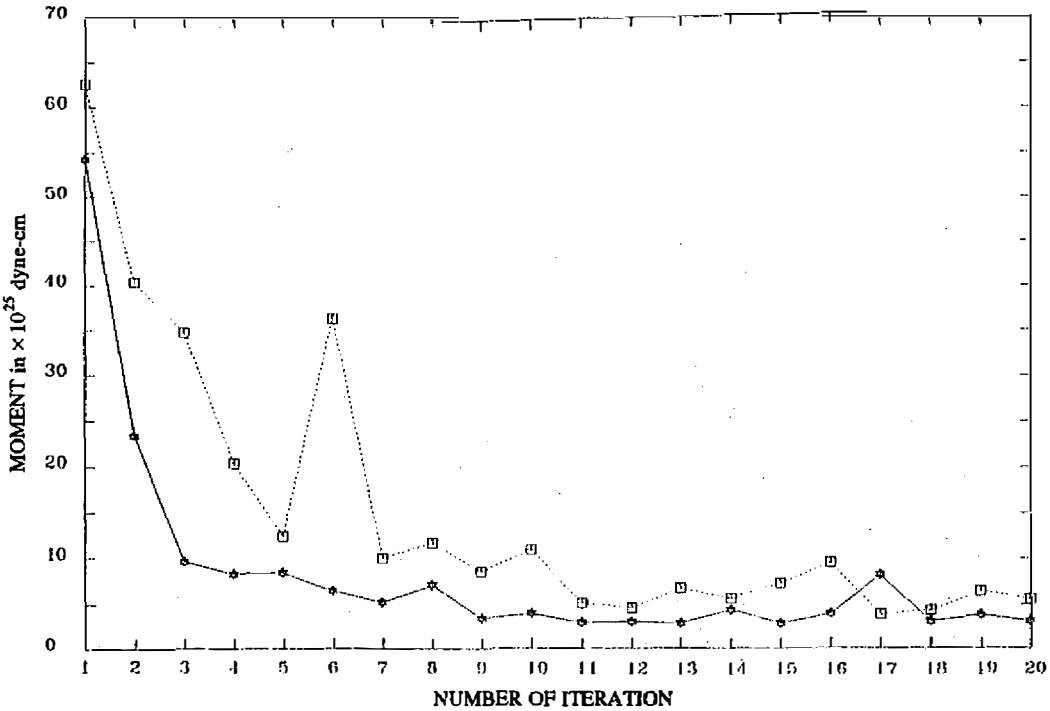

Fig. 10. Variations of seismic moment in terms of number of iteration: 'solid line with star' for Pacific data set and 'dotted line with square' for Eurasian data set.

and the amount of seismic moment. It is difficult to determine which subevents are due to refracted and reflected signals. In our case, as shown in Figure 10, the major released energy is attributed to the largest three subevents through 20 iterations. They are summed up to 8.76×10^{26} *dyne-cm* and 1.38×10^{27} *dyne-cm* for the data of Pacific stations and those of Eurasian stations, respectively. The former is almost the same as that obtained by Giardini *et al.* (1985), but the latter is about 1.6 times the former. We have assumed that the seismograms recorded at Eurasian stations, which are situated on the continental crust, would consist of more reflected and/or refracted signals, thus yielding larger value of seismic moments.

As described in the previous section, the result inverted from the data of four Pacific stations based on Pezzopane and Wesnousky's source parameters seems to be better than that from the data of Eurasian stations for the Lanhsu earthquake.

The aftershocks with $M_D > 3.0$ during nine days after the mainshock and the inverted subevents are shown in Figure 11. It is obvious that aftershocks are located at the unbroken area in the mainshock rupture sequence. Most larger aftershocks with $M_D > 4.0$ are located at the shallower part of the fault plane and are not close to the main broken zone of the mainshock. This seismicity pattern is reasonable: the mainshock occurs at the deeper part and aftershocks take place at the shallower part.

According to the asperity concept (Kanamori and Stewart,1976), the main fractured

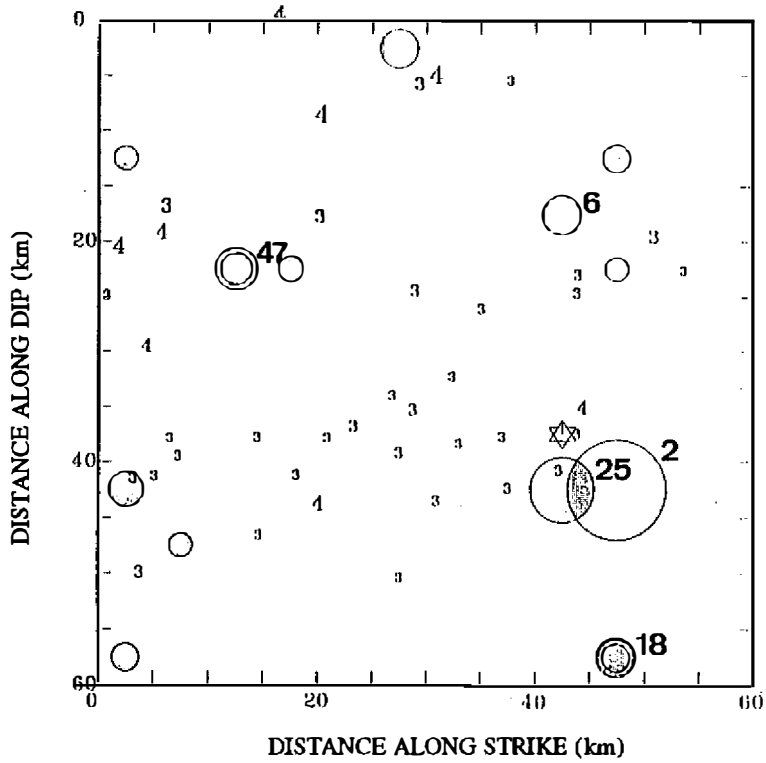

Fig. 11. Spatial distribution of mainshock rupture events (in shaded circles) and aftershocks (in integers to represent their duration magnitudes).

zone during the mainshock is regarded as a strong asperity with a breaking strength higher than a critical value. This zone breaks when the accumulated stress is greater than the critical state. Aftershock activity is related to the mainshock rupture through a certain mechanism, for instance stress corrosion as indicated by Yamashita and Knopoff (1987). They proposed two models to interpret aftershock activity. In the first model, aftershocks are assumed to be caused by subsequent slip on asperities of a fault which are locked during the fracture in the mainshock. In the second one, aftershocks are caused by a catastrophic coalescence of small fractures with the fracture surface of the mainshock. Stress corrosion cracking is assumed to be the cause of aftershock activity for both models. In Figure 11, the first model is applied to interpret aftershock activity in the case where the small subevents inverted from the seismograms are also considered to be a part of the mainshock. On the other hand, the second model works as these small subevents are considered to be aftershocks which immediately occurred after the mainshock or 'ghost' events through the inversion process due to the contamination of reflected and/or refracted waves.

Mendoza and Hartzell (1988) also mentioned that the spatial distribution of aftershocks reflects either a continuation of slip in the outer regions of the areas of maximum coseismic displacement or the activation of subsidiary faults within the volume surrounding the boundaries of the mainshock rupture.

7. CONCLUSION

Kikuchi and Kanamori's method has been used to analyze the spatio-temporal distribution of subevents of the July 23, 1978 Lanhsu earthquake based on two sets of source parameters and data from different stations in this study. Results show that the source parameters by Pezzopane and Wesnousky (1989) are more suitable in the interpretation of the observed seismograms recorded at seven stations than those by Lee and Tsai (1981). The focal depth of the earthquake is considered to be about 26 *km* rather than 6 *km* as determined by Lee and Tsai (1981) from local data. According to Pezzopane and Wesnousky's source parameters, the spatio-temporal pattern inverted from Pacific data is more reasonable than that from Eurasian data based on the distribution of subevents and errors. The optimal mainshock rupture sequence inverted from Pacific data consists of a main event, which is located near the hypocenter determined by Pezzopane and Wesnousky (1989) and has the maximal slip at 2 *sec.* after rupture and numerous subevents. The largest subevent is closed to the main event and takes place about 23 *sec.* after the main event. Smaller subevents are located far from the main event. The total value of seismic moment of the main event and two larger subevents is 8.76×10^{26} *dyne-cm.*

Acknowledgements The main part of this work was finished while the first author (N.P. Chou) was a graduate student in the Institute of Geophysics, National Central University. Numerous beneficial suggestions from Drs. Y.H. Yeh, B.Y. Kuo, Y.T. Yeh and G.K. Yu are much acknowledged. The authors would like to thank Ms. Y.L. Yeh for her aid in programming. Computing facilities were provided by the National Central University and the Institute of Earth Sciences, Academia Sinica. This study was supported by Academia Sinica and the National Science Council under Grant No. NSC 79-0202-M001-06.

REFERENCES

Aki, K. and Richards, P.G. (1980) *Quantitative Seismology: Theory and Methods*, W. Freeman Cooper, San Francisco, Calif. 932 pp.

Barrier, E. and Angelier, J. (1986) Active collision in eastern Taiwan: The Coastal Range, *Tectonophys.*, **125**, 39-72.

Giardini, D., Dziewonski, A.M. and Woodhouse, J.H. (1985) Centroid moment tensor solutions for 113 large earthquakes in 1977-1980, *Phys. Earth Planet. Inter.*, **40**, 259-272.

Kanamori, H. and G.S. Stewart (1976) Seismological aspects of the Guatemala earthquake of February 4, 1976, *J. Geophys. Res.*, **83**, 3427-3434.

Kikuchi, M., and Fukao, Y. (1985) Iterative deconvolution of complex body waves from great earthquakes -the Tokachi-Oki earthquake, 1968, *Phys. Earth Plant. Inter.*, **37**, 235-248.

Kikuchi, M. and Fukao, Y. (1987) Inversion of long-period P waves from great earthquakes along subduction zones, *Tectonophys.*, **144**, 231-247.

Kikuchi, M. and Kanamori, H. (1982) Inversion of complex body waves, *Bull. Seism. Soc. Am.*, **72**, 491-506.

Kikuchi, M. and Kanamori, H. (1986) Inversion of complex body waves II, *Phys. Earth Plant. Inter.*, **43**, 205-222.

Lee, T.Q. and Tsai, Y.B. (1981) A study of the July 23, 1978 Lanhsu, Taiwan earthquake sequence, *Bull. Inst. Earth sci:, Acad. Sin.*, **1**, 31-50.

Lundgren, P.R., Okal, E.A and Stein, S. (1988) Body-wave deconvolution for variable source parameters: application to the 1978 December 6 Kuriles earthquake, *Geophys. J.*, **94**, 171-180.

Mendoza, C. and Hartzell, H. (1988) Aftershock patterns and main shock faulting, *Bull. Seis. Soc. Am.*, **78**, 1438-1449.

Pezzopane, S.K. and Wesnousky, S.G. (1989) Large earthquakes and crustal deformation near Taiwan, *J. Geophys. Res.*, **94**, 7250-7264.

Tsai, Y.B. (1986) Seismotectonics of Taiwan, *Tectonophys.*, **125**, 17-37.

Yamashita, Y. and L. Knopoff (1987) Models of aftershock occurrence, *Geophys. J. R. astr. Soc.*, **91**, 13-26.

Young, C.J., Lay, T. and Lynnes, C. (1989) Rupture of the 4 February 1976 Guatemalan earthquake, *Bull. Seism. Soc. Am.*, **79**, 670-689.

一九七八年七月二十三日蘭嶼地震震源破裂過程之研究

周念平
中央大學地球物理研究所

王錦華
中央研究院地球科學研究所

摘　要

本研究是以七個世界網所收錄的遠場長週期 P 波記錄，來分析一九七八年七月二十三日蘭嶼地震震源破裂之過程。分析方法是 Kikuchi and Kanamori (1982, 1986) 所發展的逆推技術。此方法的基本原理是以最小二乘法的迭代技巧，在合成震波波形與觀測記錄具有最大相似時，求取破裂在時間與空間上的分佈。結果顯示此次地震之破裂主要發生在 Pezzopane and Wesnousky 所求得的震源附近，此外在地表附近以及斷層底部皆有幾個較小的次破裂發生；進一步將主震破裂事件與餘震分佈相比對，顯示餘震皆發生在主震未破裂之區域內，反應出應力在震源區於主震發生後有再分配的情形。由最大的三個破裂所累積的地震矩爲 8.76×10^{26} 達因—公分。